Relaxational dynamics after the quench of a conserved system with a continuous symmetry

M. Mondello* and Nigel Goldenfeld
Department of Physics and Materials Research Laboratory, University of Illinois at Urbana-Champaign, 1110 West Green Street, Urbana, Illinois 61801
(Received 27 August 1992)

We study the dynamics of a two-dimensional system with complex conserved order parameter, following a deep quench. In accordance with a recent theoretical prediction, we observe an effective value of the dynamical exponent at late times of $\phi=0.245\pm0.010$. While interesting dynamical effects were noticed in the study of the equal-time correlation functions, no evidence of multiscaling behavior was found. A correspondence between the quenched dynamics of this system in two dimensions and the dynamics of roughening of crystal-vapor interfaces is pointed out. We also study the dynamics in one dimension and find that $\phi\approx0.18$.

PACS number(s): 64.60.Ht, 67.40.Vs, 64.60.Cn, 64.60.My

I. INTRODUCTION

Scaling phenomena are often observed during the approach to equilibrium [1]. The classical example is spinodal decomposition of a binary alloy, where the system proceeds to its final state of two-phase coexistence through the development of a pattern characterized by a single time-dependent length scale λ. It has been found that λ varies with time t according to $\lambda(t)\sim t^{\phi}$, where the dynamical exponent $\phi=\frac{1}{3}$ for the case of a conserved order parameter and $\phi=\frac{1}{2}$ for the case of a nonconserved order parameter [2,3]. These results do not seem to depend upon the dimension D of the system, above its lower critical dimension. Furthermore, the order-parameter dynamical scattering function is found to obey a scaling law

$$S(k,t)=\lambda(t)^{D}\Phi(k\lambda(t)) , \tag{1.1}$$

where $\Phi(x)$ is referred to as a scaling function. Considerable analytical and numerical work has recently being devoted to the study of relaxation dynamics in systems with a continuous symmetry [4–13]. Previously, we investigated the relaxation dynamics of a system with a nonconserved complex (i.e., two-component, $n=2$) order parameter in two [8] and three dimensions [9], in order to address the issue of the effect of the continuous symmetry of the order parameter [O(2)] and the associated topological defects (vortices) on the relaxation process. We have also extended our investigation, introducing a vector gauge field in our model, to consider the case of the ordering dynamics of a charged system (i.e., a superconductor [10].

In this paper we study the dynamics of a two-dimensional system with complex conserved order parameter following a deep quench. There is considerable theoretical interest in systems with continuous symmetry ($n>1$) and conserved dynamics because, in accordance with a recent theoretical prediction [5,6], the growth exponent ϕ is expected to be $\frac{1}{4}$ rather than $\frac{1}{3}$, as found in systems with conserved dynamics and discrete symmetry ($n=1$). Furthermore, Coniglio and Zannetti [7] have reconsidered the quenched dynamics of the spherical model [O($n=\infty$)] and, while their results for the nonconserved case agree with previous findings, they point out the existence of two competing length scales in the conserved case associated, respectively, with the wave vector of the peak position ($k_m\sim t^{-1/4}$) and with the peak width ($k_\sigma\sim[t/\ln(t)]^{-1/4}$) of the scattering function [7]. This violates ordinary dynamical scaling although the numerical corrections might not be easy to ascertain in the usual rescaling plot. The most dramatic change from ordinary scaling, though, is that, asymptotically, the different components of the scattering function $S(k,t)$ have different rescaling exponents

$$S(t,k)\sim[M_0^2k_m^{2-D}k_\sigma^{2}]^{\phi(k/k_m)} , \tag{1.2}$$

where $\phi(x)=1-(x^2-1)^2$. The authors term this phenomenon multiscaling, since it involves infinitely many growth exponents, and they suggest it might be a generic feature of any system whose asymptotic evolution is controlled by a pair of lengths, both diverging although in a "marginally" different way. In a recent work on the O(n) models with conserved order parameter, Bray and Humayun [14] have argued that multiscaling is asymptotically ($t\to\infty$) satisfied only for $n=\infty$. If we take the asymptotic limit before the $n\to\infty$ limit, ordinary scaling is recovered. It is therefore important to try to understand what relevance this might have for systems with n finite. In particular, Bray and Humayun's argument leaves open the possibility that for large values of n one might still be able to observe multiscaling-type behavior at intermediate times [14].

In the present numerical study, we observe an effective value of the dynamical exponent at late times of $\phi=0.245\pm0.010$, which confirms Bray's theoretical prediction [5]. As in the conserved scalar case [15] we do not find convincing evidence for multiscaling, although the study of the correlation functions exhibits a number of interesting dynamical effects. Systems that, in contrast to the present one, cannot support stable defects may be a

more appropriate testing ground for (asymptotic or transient) multiscaling.

Apart from its theoretical significance, the system here investigated has intrinsic physical interest because of the relation between its ordering dynamics and the roughening dynamics of crystal-vapor interfaces, which we propose in Sec. VI. This may lead to a direct experimental test of the theoretical predictions.

The organization of this paper is as follows. In Sec. II we describe how the conservation constraint is imposed in the cell dynamical system (CDS) version of our model. The time dependence of the ordering process is discussed in Sec. III. Section IV considers the evidence for dynamical scaling, while the question of multiscaling is directly addressed in Sec. V. In Sec. VI we introduce a correspondence between our model, in two dimensions, and the solid on solid (SOS) model of a vapor-crystal interface and discuss possible experimental implications of our results. Section VII is devoted to an illustration of the ordering dynamics of a one-dimensional system. We summarize our conclusions in Sec. VIII.

II. MODEL

We consider a complex conserved order-parameter field on a $L \times L$ lattice in two dimensions. The evolution of the order-parameter field $\Psi(\mathbf{r},t)=X(\mathbf{r},t)+iY(\mathbf{r},t)$ is governed by the same phenomenological equation (Cahn-Hilliard equation) as in the case of a system with discrete symmetry:

$$\frac{\partial \Psi(\mathbf{r},t)}{\partial t}=M\nabla^2\left[\frac{\partial F(\Psi(\mathbf{r},t))}{\partial \Psi^*(\mathbf{r},t)}\right], \tag{2.1}$$

where M is a kinetic coefficient, assumed to be independent of Ψ, and

$$F\{\Psi(\mathbf{r},t)\}=\int d^2\mathbf{r}\left[|\nabla\Psi(\mathbf{r},t)|^2-a|\Psi(\mathbf{r},t)|^2+\frac{b}{2}|\Psi(\mathbf{r},t)|^4\right]. \tag{2.2}$$

The coefficients a and b are positive after the quench. We performed the simulations using the cell-dynamics scheme [16]. In this scheme we can, in principle, choose different length scales for the isotropic Laplacian averaging and the range of the conservation constraint. In practice, we have limited both the isotropic averaging and the conservation constraint to nearest-neighbor ($\langle \mathrm{NN}\rangle$) and next-nearest-neighbor ($\langle \mathrm{NNN}\rangle$) sites ($\mathbf{m}$). To implement the dynamics of the system, we first evolve the components of the order parameter, at site $\mathbf{n}$ and time step t, as in the nonconserved case [8]:

$$\begin{aligned}X'(\mathbf{n},t+1)&=A\tanh[R(\mathbf{n},t)][X(\mathbf{n},t)/R(\mathbf{n},t)]\\&\quad+C[\langle\langle X(\mathbf{n},t)\rangle\rangle-X(\mathbf{n},t)],\\Y'(\mathbf{n},t+1)&=A\tanh[R(\mathbf{n},t)][Y(\mathbf{n},t)/R(\mathbf{n},t)]\\&\quad+C[\langle\langle Y(\mathbf{n},t)\rangle\rangle-Y(\mathbf{n},t)],\end{aligned} \tag{2.3}$$

where $R(\mathbf{n},t)=|\Psi(\mathbf{n},t)|$ and

$$\langle\langle \psi(\mathbf{n},t)\rangle\rangle\equiv\sum_{\langle \mathrm{NN}\rangle}\left[\frac{\psi(\mathbf{m},t)}{6}\right]+\sum_{\langle \mathrm{NNN}\rangle}\left[\frac{\psi(\mathbf{m},t)}{12}\right]. \tag{2.4}$$

Here A gives a measure of the depth of the quench and C controls the coupling strength of the cells. We then impose a local conservation constraint on the intermediate values $X'(\mathbf{n},t+1)$ and $Y'(\mathbf{n},t+1)$ of each separate component:

$$\begin{aligned}X(\mathbf{n},t+1)&=X(\mathbf{n},t)=\langle\langle X'(\mathbf{n},t+1)-X(\mathbf{n},t)\rangle\rangle,\\Y(\mathbf{n},t+1)&=Y(\mathbf{n},t)-\langle\langle Y'(\mathbf{n},t+1)-Y(\mathbf{n},t)\rangle\rangle,\end{aligned} \tag{2.5}$$

where $\langle\langle\cdots\rangle\rangle$ is defined as in Eq. (2.4). For our simulations, we apply periodic boundary conditions and choose $A=1.3$ and $C=0.5$. Random initial conditions were also chosen, as in the nonconserved case, and the same topological considerations discussed in Ref. [8] apply here. Since, even in the presence of conservation, the lowest-energy state of the system is vortex-free, the ordering process proceeds through vortex-pair annihilation. Qualitatively, we observe that at early times the density of vortices is over one order of magnitude higher than in the nonconserved case and that at least in the absence of noise, finite systems are very likely to "freeze" in metastable states at late times, as we have observed in systems of small size ($L=32$). The freezing, we suggest, is caused by the presence of a great number of local minima of the system energy functional that satisfies the global conservation constraint

$$\int d^2\mathbf{r}\,\Psi(\mathbf{r},t)=\text{const}, \tag{2.6}$$

where, for random initial conditions, const≈ 0. For systems of the size used in this work ($L=256$), we do not see any sign of freezing in the time range considered ($100<t<208\,100$).

III. DYNAMICS AND POWER-LAW BEHAVIOR

We now turn to a quantitative discussion of the dynamics. There are several *a priori* independent characteristic length scales in the system. The first two moments ($\bar{k}_1$ and $\bar{k}_2$) of $S(k,t)$, the circularly averaged time-dependent scattering function [17],

$$\bar{k}_m(t)=\frac{\int_0^\infty dk\,k^m S(k,t)}{\int_0^\infty dk\,k^{m-1}S(k,t)},\quad m=1,2, \tag{3.1}$$

define two characteristic length scales $\lambda_m(t)=L/[2\pi\bar{k}_m(t)]$, $m=1,2$. Alternatively, we can use the average intervortex spacing defined as $d(t)=L/\sqrt{N(t)}$, where $N(t)$ is the number of vortices remaining at time t. Finally, as a characteristic length associated with the real-space correlation function of the order parameter

$$C(r,t)\equiv\frac{\langle\Psi^*(r,t)\Psi(0,t)\rangle}{\langle\Psi^*(0,t)\Psi(0,t)\rangle},$$

we use its first zero $r_0(t)$, which is the shortest length that satisfies the relation $C(r_0(t),t)=0$. As shown in Fig. 1, our data for $r_0(t)$ and $\lambda_1(t)$ are consistent with an asymptotic power-law behavior $\lambda(t)\sim t^{0.245\pm0.010}$. There is a

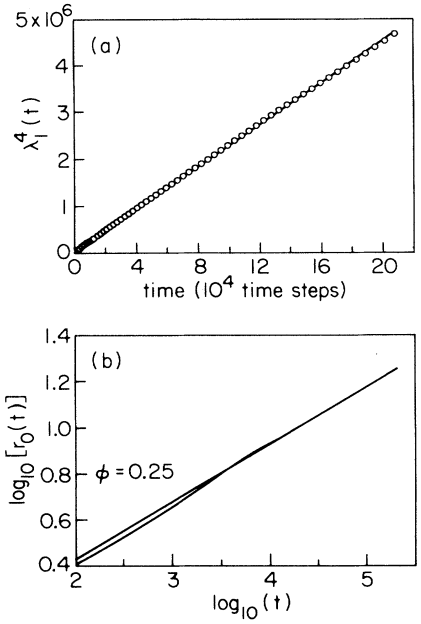

FIG. 1. Graphs of λ_1^4 vs t (a) and $\log_{10}(r_0)$ vs $\log_{10}(t)$ (b). A straight line is drawn for comparison in (a), where statistical fluctuations are also shown whenever larger than the symbol size. The slope of the straight line in (b) is 0.25. Statistical averages were taken over 40 initial conditions.

slight difference between the length scales associated with the first and second moment of the scattering function: $\lambda_2(t)$ is better fitted by $[t/\ln(t)]^{1/4}$, suggesting the possible presence of a second, somewhat slower, length scale in the system (Fig. 2). It should be stressed, however, that an unambiguous determination of a systematic logarithmic correction to the power-law behavior is beyond the "resolving power" of the present numerical data and any interpretation of this result in terms of multiscaling should be taken with caution (cf. the scaling analysis of the scattering function below). Bray has suggested that the scaling form for the real-space correlation function explicitly depends on the equilibrium modulus M of the order parameter as [6]

$$C(r,t)=M^2\Gamma(r(M^2/t)^{1/4}) .$$

Identifying M with the time-dependent spatial average of $|\Psi(\mathbf{n},t)|$, we have also tried to fit the data rescaling time as $t/\langle\Psi^*(t)\Psi(t)\rangle$. Although the high density of vortices makes this correction significant at early times, it does not appreciably modify the overall time behavior of the system and it cannot explain the difference in time dependence of the different length scales.

Note that the clear-cut distinction between the values and statistical properties of the first and second moment of the scattering function, which is typical of nonconserved systems [8], does not apply to the conserved case. This is because the main contributions to the integrals of the different moments come from finite k components of the scattering function rather than $k=0$.

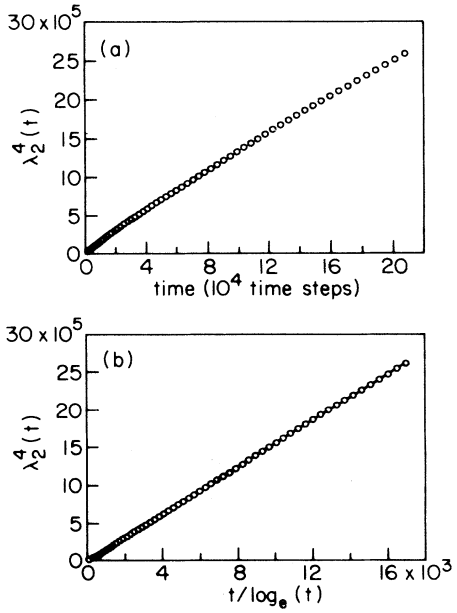

FIG. 2. Comparison of λ_2^4 vs t (a) and λ_2^4 vs $[t/\log_e(t)]$ (b). A straight line is drawn for comparison in (b). Statistical averages were taken over 40 initial conditions and statistical fluctuations are shown whenever larger than the symbol size.

IV. DYNAMICAL SCALING

The scaling of the scattering function presents some interesting features. We have tried to rescale it using both its first and second moment. This is of interest because of the slight difference, noted above, in the time dependence of the two associated length scales. As shown in Fig. 3,

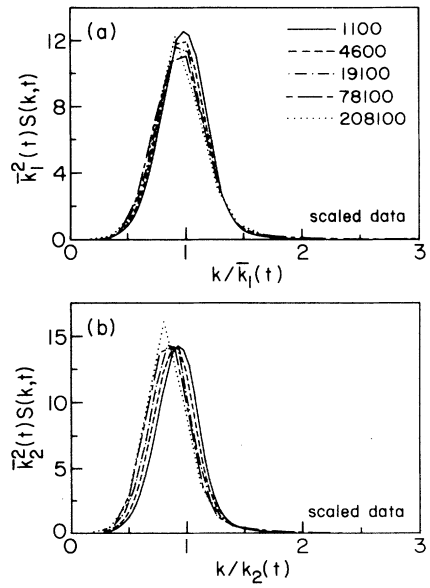

FIG. 3. Comparison of two possible rescalings for the scattering function $S(k,t)$, using $\bar{k}_1$ (a) and $\bar{k}_2$ (b). The lines are linear interpolations of the data points taken on 256×256 lattices at 1100 (solid line), 4600 (dashed line), 19 100 (chain-dotted line), 78 100 (chain-dashed line), and 208 100 (dotted line) time steps. We averaged over 40 initial conditions.

we find that the first moment gives the best overall agreement, but it is worth noticing that while $\bar{k}_1$ seems to accurately describe the evolution of the peak position of the scattering function, $\bar{k}_2$ appears to give a more accurate representation of the increase in the peak height. This is reminiscent of the behavior found in the $n=\infty$ case, due to the presence of two (logarithmically) different length scales [7]. Here, however, the wavelength associated with the peak position (m), $\lambda_m(t)=2\pi/\bar{k}_m(t)$, increases faster than the rescaling length for the peak height, while the opposite is true in the $n=\infty$ case. This trend holds true for all the curves shown in Fig. 3, except the one corresponding to the latest time considered. Looking at the unscaled data (Fig. 4), it is clear that, at this late time, the peak half-width of the scattering function is comparable with the circular-averaging "bin" in k space, so that it is possible that finite-size effects are masking the exact location and height of the peak.

Looking at the log-log plot of the rescaled scattering function, Fig. 4, $\bar{k}_1^{-2}(t)S(k,t)=\Phi(x)$, we see that at small $x=k/\bar{k}_1<1$ it satisfies Yeung's inequality [18], $\Psi(x)\leq x^4$, while for $x>1$, it appears to approach asymptotically x^{-4}. This last trend is not as well defined here as in the nonconserved case, but we suggest that this is due to the specific features that the conservation law imposes on the scattering function. Shinozaki and Oono [19], in particular, noticed a hump (at $x=3$) in the log-log plot of the scattering function for the conserved scalar case in three dimensions: the same effect might also be present here, although our data are not as definite in this regard. In any case, all of the "dynamical structure" of the rescaled scattering function, that is, the features that depend on the conservation law, should be confined to values of x of order unity or smaller, while dynamical scaling should asymptotically extend to $x\gg 1$. In this region, the dominant factor should then be the local configuration of the order parameter, which only depends on the symmetry (the defect topology) and the static balance of the elastic energy. We expect therefore that the universal function should asymptotically decay as x^4, due to the vortex-field configuration. This expectation is borne out by the small $y=r/r_0(t)$ behavior of the rescaled real-space correlation function $C(r,t)=\Gamma(y(t))\approx 1-y^{\psi}$, where $r_0(t)$ is the position of the first zero of $C(r,t)$ and $\psi=1.6\pm 0.05$ (see inset of Fig. 5), as in the nonconserved case [8,9]. Recent analytic work by Bray and Puri [12] and, independently, Toyoki and Liu and Mazenko [13], appears to confirm the presence of an anomaly for (nonconserved) systems with $n=2$ ($D>1$). They report that the exponential is non-Gaussian due to a logarithmic correction and, in the small x limit, Toyoki finds

$$\Gamma(x)=1-[\ln(2)-\tfrac{1}{4}-\tfrac{1}{2}\ln(x)]x^2 ,$$

which is numerically close to $\approx 1-x^{1.6}$ at a representative short distance, as shown in Fig. 1 of Ref. [13(a)]. A corresponding logarithmic correction is found in the $r\to 0$ limit of the correlation function of an isolated vortex configuration, confirming the principal role of defects in the origin of this anomalous behavior. As shown in Fig. 5, the data for the order-parameter correlation function appear to collapse onto a universal curve over virtually the entire time range considered, showing that this function is rather insensitive to the finite-size and possible transient effects (see below) we have observed in other

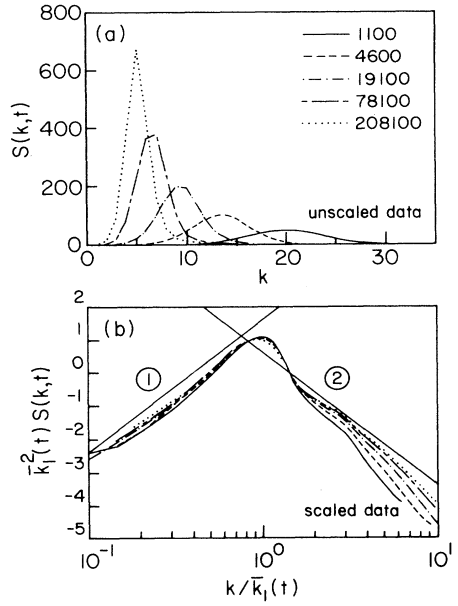

FIG. 4. We give here the unscaled data for the scattering function $S(k,t)$ (a) and the log-log plot of the same data rescaled with $\bar{k}_1$ (b). In (b), we show, for comparison two lines representing $\sim(k/\bar{k}_1)^4$ and $\sim(k/\bar{k}_1)^{-4}$ power-law behavior. Here we have adopted the same symbols and conventions of Fig. 3.

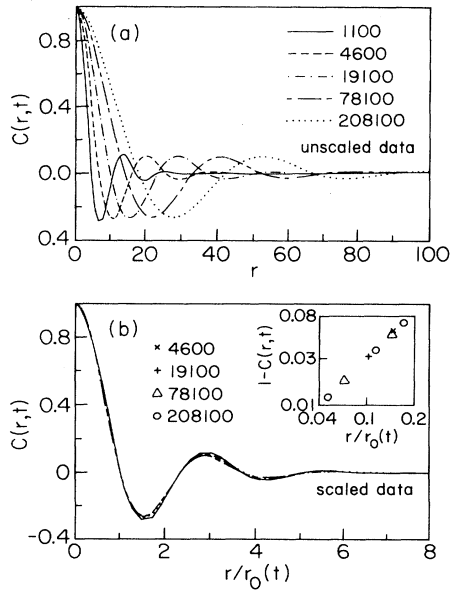

FIG. 5. Demonstration of dynamical scaling for $C(r,t)=\Gamma(r/r_{1/2}(t))$, where $r_{1/2}(t)$ is the half-width of $C(r,t)$. Here we have adopted the same symbols and conventions of Fig. 3. Inset is a log-log plot of $1-\Gamma(x)$ in the limit of small x. The diagonal of the inset square has a slope of 1.6.

correlation functions.

Considering now the behavior of the real-space correlation functions of the vortices we find remarkable differences with respect to the results obtained in the nonconserved case. In particular, here we observe a *dynamical asymmetry* between the radial correlation function of vortices of equal sign $C_{nn,pp}(r,t)$, that, as can be seen in Fig. 6, shows a small but systematic deviation from scaling, and the correlation function of vortices of opposite sign $C_{np,pn}(r,t)$ where no such deviation is detectable (Fig. 7), at least in the main peak. The presence of a developing peak in $C_{nn,pp}(r,t)$ is in sharp contrast with the monotonic behavior found in the nonconserved case (Fig. 8 of Ref. [8]). We also note here the presence in both functions of a well-defined secondary peak, while no secondary peak was visible in the nonconserved case (Figs. 8 and 9 of Ref. [8]).

A full appreciation of the features in the correlation functions of the vortices would require a detailed understanding of how the conservation of the order parameter affects the "effective" interaction of a vortex-antivortex pair. This is feasible within the framework of the defect-dynamics approach [20], but we have not attempted this task here.

We can summarize the main results that have emerged from the analysis of the correlation functions as follows. (i) The vortex-field configurations at short distance are insensitive to the dynamical changes introduced by the conservation law, as shown by the fact that the small-r behavior of the correlation function of the order parameter is identical in the conserved and nonconserved case. (ii)

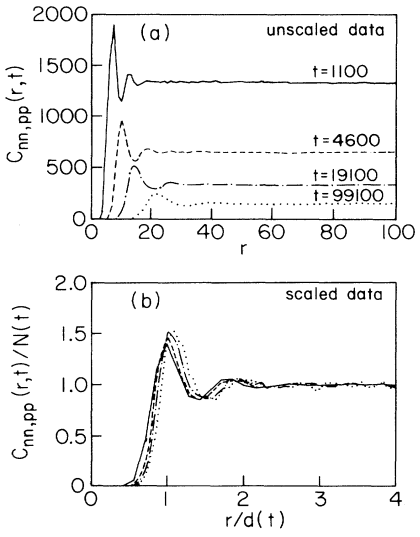

FIG. 6. Demonstration of dynamical scaling for $C_{nn,pp}(r,t)\equiv\langle n(0,t)n(r,t)+p(0,t)p(r,t)\rangle$, where n and p are the (time-dependent) local densities of negative and positive vortices, respectively. $N(t)$ is the total number of vortices in the system at time t and $d(t)=L/\sqrt{N(t)}$. The data were taken on 256×256 lattices at 1100 (solid line), 4600 (dashed line), 19 100 (chain-dotted line), and 99 100 (dotted line) time step. We averaged over 60 initial conditions.

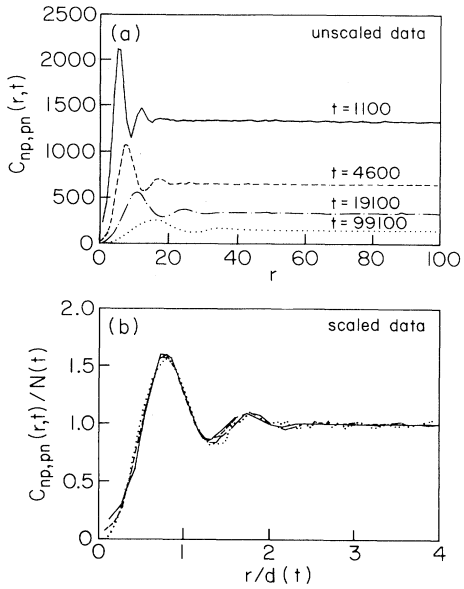

FIG. 7. Demonstration of dynamical scaling for $C_{np,pn}\equiv\langle n(0,t)p(r,t)+p(0,t)n(r,t)\rangle$. Here we have adopted the same symbols and conventions of Fig. 6.

The correlation functions of the vortices are a very sensitive probe of these same dynamical effects, as indicated by the significant differences in spatial dependence and scaling properties (pointed out above) between the conserved and nonconserved cases.

V. MULTISCALING

The question of multiscaling was addressed only indirectly in the previous section. Although evidence of possible corrections to scaling was pointed out, this, by itself, is not strong or consistent enough to justify the dismissal of the dynamical scaling hypothesis. The difficulty of finding numerical evidence for multiscaling behavior was already pointed out by Coniglio and Zannetti in their original paper [7]. They suggested a different plotting of the scattering function data that directly probes the multiscaling hypothesis: the idea that, asymptotically, the time evolution of each (k) component $S(k,t)$ of the scattering function is characterized by a different growth exponent $\phi(k/k_m)$, where $\bar{k}_m$ is the position of the peak maximum. In the thermodynamic limit, where k is the position of the peak maximum. In the thermodynamic limit, where k is a continuum variable, there are therefore infinitely many scaling exponents $\phi(x)$ (multiscaling). To find these exponents for a D-dimensional system, we need to plot

$$\ln[\bar{k}_m^{D}(t)S(\bar{k}_m(t)x,t)] \text{ versus } \ln[2\pi/\bar{k}_m(t)]\ , \qquad (5.1)$$

at constant $x=k/k_m$. This relation follows immediately from Eq. (1.2) if we ignore the (logarithmic) difference between k_m and k_σ (the peak width of the scattering function). The slope $D\phi(x)$ of this relation is expected to be a constant [$\phi(x)=1$] if the dynamical scaling relation is

satisfied while $\phi(x)=1-(x^2-1)^2$ in the O($n=\infty$) (spherical) model with the conserved order parameter studied by Coniglio and Zannetti [7].

We have performed the multiscaling analysis with the identification $\bar{k}_m(t)=\bar{k}_1(t)$. The numerical results are shown in Fig. 8, where a comparison is made with the analytic form found for $n=\infty$. We remark that the range of values (at constant x) shown in the figure does not represent statistical fluctuations, which should be superimposed to all data points. Rather, it expresses an estimate of the systematic errors involved in trying to evaluate the slope of Eq. (5.1) for values of x outside the immediate neighborhood of $x=1$, where only one value for the slope is given. The reported midrange values try, in all cases, to give an estimate of the overall slope, but we note that the more reliable values, for $x>1$, are given by the lower-range points, since they are associated with the late-time asymptotes. We also observe strong finite-size effects for $x=0.02$.

There is a clear discrepancy between the results of the numerical study ($n=2$), which are roughly consistent with $\phi(x)=$const, and the analytic results ($n=\infty$), which exhibit a strong variation with x. Thus we may conclude that ordinary scaling rather than multiscaling seems to describe the asymptotic behavior of our system. Our results are in fact similar to the results obtained for the scalar case ($n=1$) in three dimensions [15]. The absence of sharp domain boundaries in the $n=2$ case, in contrast to the scalar case, does not seem to significantly effect the asymptotic scaling behavior of our system. This result is consistent with the argument put forward recently by Bray and Humayun [14] that conventional scaling holds asymptotically for all finite n.

Regarding future directions of work, we would like to make here a more general comment. As we have seen in the previous section, the existence of topological defects with extended field configurations creates "configurational" constraints on the short rescaled-length behavior of the system and, correspondingly, severely reduces the phase space available to its evolution: we can give a fairly accurate description of the evolution of the system using only the positions of the vortices. This delicate interplay between symmetry constraints and dynamics and the possibility of long transients associated with the existence of several competing length scales makes it, in principle, particularly difficult to ascertain (asymptotic or transient) multiscaling behavior in our system. To avoid some of these difficulties, it would be worthwhile to study the relaxational behavior of systems with conserved dynamics that cannot support stable topological defects ($n>D$).

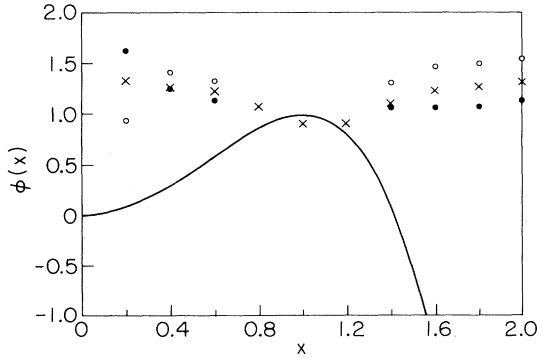

FIG. 8. Here we compare the analytic result for $n=\infty$ (solid line) and the numerical results for $n=2$. We give the best estimates of the slope of Eq. (5.1) as a function of x, using the entire time range $100<t<208\,100$ (X). Whenever there is a significant change of slope over this time range, we also give an estimate of the early-time ($100<t<10\,000$, ●) and late-time ($20\,000<t<200\,000$, ○) slopes).

VI. PROPOSED EXPERIMENTAL REALIZATION

Although we do not know if any physical system with a complex ($n=2$) conserved order parameter, it may be possible, in the spirit of universality, to apply some of the results of this chapter to the roughening dynamics of crystal-vapor interfaces [21]. The starting point of our considerations is that the equilibrium statistical mechanics of both the discrete Gaussian model of roughening (in $D=3$) and the XY model have an *exact* $D=2$ Coulomb gas representation [22]. This permits us to identify the roughening transitions of the crystal interface model with the vortex-unbinding transition of the XY model and establishes a correspondence between the static equilibrium properties of the two models. Note that in this mapping the temperature of the XY model (T_{XY}) corresponds to the inverse temperature of the crystal ($T_{\rm cr}\sim 1/T_{XY}$) so that the rough (high-temperature) phase of the crystal-vapor interface is associated with the bound (low-temperature) phase of the XY model, and both of them correspond to the screened (low-temperature) phase of the Coulomb gas. One may object that the two models are not exactly identical, since the Coulomb gas representation of the crystal-vapor interface contains, in principle, charges of any integer value q, while in XY model only the charges with $|q|=1$ are (energetically) stable. We expect, however, that only charges with $|q|=1$ are relevant at the transition since, as we decrease the temperature in the XY model (or as we increase the temperature in the crystal interface model), the $|q|=1$ charges are the last to bind, allowing the formation of the screened phase. Using renormalization-group arguments, the relation between the discrete Gaussian model and the $D=2$ Coulomb gas can be extended to more general SOS (solid-on-solid) models of the crystal-vapor interface [22].

We can now try to extend this correspondence to include the dynamical properties of the roughening transition after a "quench" in the high-temperature phase [23]. A crucial element to be considered is now the conservation of the order parameter, which can be identified with the mean-square deviation of the interface profile from its average position. We can envision two basic mechanisms for the growth of the interfacial fluctuations: evaporation condensation at the surface of the crystal, which we suppose to be in local equilibrium with its vapor phase, and surface diffusion along the solid-vapor interface. The first mechanism (evaporation condensation) will lead to a nonconserved dynamics for the order parameter, while surface diffusion satisfies a local conservation law, which we

can express as a continuity equation for the mass current at the interface [24].

These considerations suggest that the relaxational dynamics of conserved order parameter and that of a crystal surface, in the regime where surface diffusion is dominant, may be in the same dynamic universality class: they have the same symmetries and the equilibrium behavior is identical. For this mapping to apply to the relaxational dynamics, we would not only need to demonstrate that the dynamics is controlled by a renormalization-group fixed point (presumably a zero-temperature fixed point such as that which Bray considered), but also show explicitly that there are no other hydrodynamic modes relevant at this fixed point for the relaxational dynamics of a crystal surface. This is beyond the scope of the present work, but should certainly be investigated in the future. It is natural to extend this analogy to the nonconserved complex order-parameter dynamics, which should therefore correspond with the relaxational dynamics of a crystal surface, in the regime when evaporation condensation is dominant.

This hypothesis implies that there are two different dynamical exponents ϕ for the growth of fluctuations in the rough phase: when the growth is due to evaporation condensation we expect $\phi=\frac{1}{2}$, and when the dominant mechanism is surface diffusion we expect $\phi=\frac{1}{4}$. Since both mechanisms are bound to be present in any real physical system, one may think that evaporation condensation (leading to the faster growth) will always dominate the asymptotic regime, but the crucial question, experimentally, is *when* the crossover occurs.

The formation of thermal grooves ($\sim 0.1-1.0$ μm in depth) during polycrystal sintering offers one example of the competition between these two mechanisms [25]. In this process, interfacial fluctuations nucleate at surface grain boundaries and lead to smooth self-similar interface profiles (grooves) whose characteristic length grows in time. This is of course quite different from the case of roughening, which does not depend on heterogeneous nucleation and only leads to *statistically* self-similar patterns. These differences, however, may not be as important as the role played by the conservation law in the dynamics of the system, and we can also think of the formation of thermal "grooves" as an intermediate stage in the roughening process.

For our purposes, the most interesting aspect of the growth process of thermal grooves is the range of experimental situations available. Depending on the material and annealing procedure chosen, the contribution of surface diffusion may be ignored from the first few minutes after the quench or, at the opposite extreme, it may dominate the process for hours or even days. It is worthwhile to notice that surface diffusion leads, at least in this case, to a $t^{1/4}$ growth law and evaporation condensation to a $t^{1/2}$ law [25], in agreement with the proposed correspondence and with our numerical results for the O(2) model.

Mullins considered the relaxation dynamics of *macroscopic* perturbations (>10 μm) on solid surfaces [26]. Above the roughening temperature, he found that sinusoidal perturbations of wavelength λ decay exponentially (keeping their shape) with characteristic times proportional to λ^2 and λ^4 when evaporation condensation or, respectively, surface diffusion is the controlling mechanism. These results were obtained within a linearized hydrodynamic theory, so that the decay of any initial surface configuration reduces to the decay of its Fourier components. If the decay time (τ) of the sinusoidal component of wave length λ is $\tau\sim\lambda^n$, only components with $\lambda>t^{1/n}$ will survive after a time t: i.e., $\lambda(t)\sim t^{1/n}$ is the characteristic size of smooth regions at time t.

Beside evaporation condensation and surface diffusion, transport through the bulk offers another possible mechanism for surface dynamics [26]. This is quite different from the previous two, however, because it subordinates the dynamics of the surface to the (conserved) dynamics of the bulk. It is not too surprising, therefore, that when the dynamics is controlled by bulk diffusion, a sinusoidal surface of wavelength λ decays exponentially, above the roughening temperature, with a characteristic time proportional to λ^3.

The prediction of a $\frac{1}{4}$ exponent for the roughening dynamics in the presence of conservation should be contrasted with a previous proposal by Villain [27]. Using a microscopic model of the smoothening process of a crystalline surface after a quench below the roughening temperature (the inverse process to the roughening dynamics considered above), he finds that if the process is dominated by surface diffusion, the linear dimension (R) of smooth domains grows a $R(t)\sim t^{1/3}$. To reconcile the two predictions, one should assume that there is a dynamical asymmetry between the smoothing and roughening processes. While this is not obvious for conserved dynamics, since in this case the two processes are both controlled by long-range surface diffusion, such an asymmetry is certainly present in the nonconserved case. After rapidly raising the temperature into the disordered phase of a nonconserved system (crystal smoothing when evaporation condensation is dominant), the growth of "disorder" (smooth surfaces) should be much faster than any power law because in this case, nearest-neighbor interactions are completely ineffective and there is no more distinction between global and local equilibrium: i.e., the relaxation is controlled by the local dynamics (local cell dynamics in the CDS scheme).

To make clear the importance of crystalline order for the previous results on roughening dynamics, it is worth mentioning the corresponding results for fluids. For a $D=3$ fluid ($D=2$ interface) the "roughening" temperature is $T=0$, that is, the width of the liquid-vapor interface diverges (in the thermodynamic limit) for any finite temperature, and the growth of the order parameter (mean-square deviation of the interface profile) is predicted to be $\sim\sqrt{\ln(t)}$ for both the conserved and conserved case [28].

VII. ONE-DIMENSIONAL SIMULATIONS

We have performed one-dimensional simulations of the quenched dynamics of a conserved complex order parameter on a lattice of size $L=4096$. The corresponding CDS equations are formally identical to the ones used in two dimensions, except that the Laplacian averaging and

the conservation constraint now affects only the two nearest neighbors. In these simulations we have used $A=1.3$ and $C=0.25$ [cf. Eqs. (2.3)–(2.5)]. A linear stability analysis (see Appendix) shows in fact that for $A=1.3$ the upper limit of linear stability of the CDS model in one dimension is $C=0.27$. For values of C (≥ 0.4) a numerical instability occurs, while at intermediate values, such as $C=0.3$, the algorithm appears stable, but a progressive slowing down of the ordering dynamics is noticed in the longer simulations: a possible indication that short-wave structures (a sign of weak instability) are developing in the system, interfering with the formation of large scale patterns. We should point out that in one dimension there are no localized defects in the system, but because of periodic boundary conditions (PBC), there is a conserved winding number $N_w \sim \sqrt{L}$ associated with the initial conditions. In fact, the algebraic sum of the phase differences ($\Delta\theta$) between nearest-neighbor vectors on a lattice loop (PBC) is a multiple of 2π and becomes, asymptotically, a constant [29]. This means that the order parameter cannot be completely untwisted, so that the effective size of the system is $L_{\text{eff}} \sim L/N_w \sim \sqrt{L}$, the period of the maximally ordered state compatible with the conservation of N_w. In the case studied, this would correspond to $L_{\text{eff}} \approx 64$. At the end of the present simulations, after 3×10^5 time steps, the typical size of the ordered domains, as measured from the first zero of the order-parameter correlation function, is $\lambda \approx 7$, so that we do not expect finite-size effects to be dominant.

To monitor the growth of order in the system, we have used the first moment of the scattering function $[k_1(t)]$ and the first zero of the real-space correlation function of the order parameter $[r_0(t)]$. The results were obtained averaging over 20 initial conditions. As shown in Fig. 9, we find for both length scales $\lambda \sim t^{0.18\pm 0.01}$. This result seems incompatible with a $\phi=\frac{1}{4}$ exponent, as suggested by Bray for higher dimensional systems, but leaves open the possibility of a $\frac{1}{6}$ or slightly smaller rational exponent. Newman, Bray, and Moore [30] have shown that the one-dimensional system with complex nonconserved order parameter is special due to the linearity of its equations of motion (when written in terms of the phase variable), so that we should not expect Bray's general renormalization-group argument [5,6] (which predicts $\phi=\frac{1}{4}$) to apply to the conserved version of the same system. At present, we do not know of any firm theoretical predictions for the case considered.

No systematic attempt was made to study the dynamical scaling of the correlation functions in this case. Nevertheless, we have observed a significant time dependence (increase) of the first minimum of the rescaled order-parameter correlation function $C(r,t)=\Gamma(r/r_0(t))$ up to at least 4×10^4 time steps. This contrasts with the fast convergence to a universal curve observed in two dimensions, but a comparison with the two-dimensional case must take into account not only the different growth exponents ϕ, but also the different values of C used in the two cases. In the time range considered, the slow dynamics allows us to probe the $x=r/r_0(t)\to 0$ limit of $\Gamma(x)\approx 1-x^{\psi}$ only up to $x\geq 0.2$. Here we find

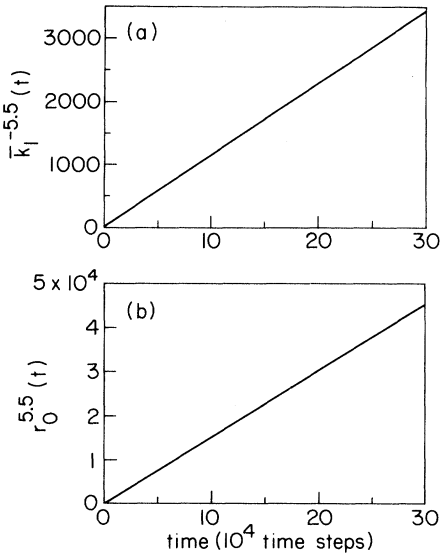

FIG. 9. Graphs of $(\bar{k}_1)^{-5.5}$ vs t (a) and $r_0^{5.5}$ vs t (b). Statistical averages were taken over 20 initial conditions.

$\psi=1.94\pm 0.05$, but there are indications that ψ has not yet attained its limit value. This result, which is compatible with a Gaussian behavior of the correlation function at small x, confirms that the result $\psi\approx 1.6$, obtained in two-dimensional systems with both conserved and nonconserved dynamics (see above and Ref. [8]), is in fact due only to the presence of vortices.

VIII. CONCLUSIONS

We have presented the results of a numerical study of the coarsening dynamics of a two-dimensional system with a complex ($n=2$) conserved order parameter. We observe an effective value of the dynamical exponent $\phi=0.245\pm 0.010$ consistent with the value of $\frac{1}{4}$ predicted by Bray using renormalization-group arguments [5,6]. The correlation function of the order parameter satisfies dynamical scaling from early times and shows an anomalous short-distance behavior identical to the one observed in the nonconserved case. We observe a *dynamical asymmetry* between the correlation function of vortices of equal sign, that, in the time range considered, show a small but systematic deviation from scaling and the correlation function of vortices of opposite sign, where no such deviation is detectable.

We have considered both ordinary dynamical scaling and multiscaling for the scattering function of the order parameter. Despite some scattering of the data, our results appear to be consistent with ordinary scaling and to exclude multiscaling, similar to the results obtained in the conserved scalar ($n=1$) case. This indicates that the absence of sharply defined domain walls does not significantly affect the asymptotic scaling behavior of the system. This result is also consistent with the recent theoretical argument by Bray and Humayun [14] that conventional scaling holds asymptotically for all finite n.

We propose a correspondence between the quenched dynamics of our system and the dynamics of roughening of a crystal-vapor interface, when surface diffusion is the dominant growth mechanism. This correspondence can be extended to the nonconserved case. Finally, some aspects of the one-dimensional system relaxation dynamics are discussed and the reduced stability of the CDS model in this case is pointed out.

ACKNOWLEDGMENTS

We thank Yoshi Oono for a number of useful discussions on multiscaling and John Stewart for his valuable insights on the crystal-vapor interface dynamics. This work was supported partially by the National Science Foundation through Grant No. DMR-89-20538 administered through the Illinois Materials Research Laboratory. We acknowledge the support of the Computer Center at the Materials Research Laboratory. One of us (M.M.) was partially supported by the National Science Foundation through Grant No. DMR-89-09232 administered through the Materials Science Department at the University of Cincinnati.

APPENDIX

Linear stability of the CDS algorithm in $D=1$

We consider here the linear stability of the one-dimensional CDS algorithm around a uniform solution ψ_0, corresponding to a stable fixed point of the cell dynamics

$$\psi(n,t+1)=A\tanh[\psi(n,t)]\equiv F(\psi(n,t)) , \tag{A1}$$

where ψ is the modulus of the order parameter $\Psi(n,t)=X(n,t)+iY(n,t)$, n is a lattice site, and A is a control parameter. Initially, we will ignore the vector character of the order parameter, since "angular" displacements turn out to lead to weaker instabilities than modulations of the spin "length" (see below).

Following closely the analogous calculation by Oono and Puri [31], we start from the (scalar) CDS algorithm for the nonconserved order parameter

$$\psi(t+1,n)=F(\psi(n,t))+C[\langle\langle\psi(n,t)\rangle\rangle-\psi(n,t)] , \tag{A2}$$

where C is a second control parameter and, in $D=1$,

$$\langle\langle\psi(n,t)\rangle\rangle\equiv\tfrac{1}{2}[\psi(n+1,t)+\psi(n-1,t)] . \tag{A3}$$

Expanding Eq. (A2) around ψ_0 $[\equiv F(\psi_0)]$ and keeping only the linear terms in $\delta(n,t)$ $[\equiv\psi(n,t)-\psi_0]$, we obtain

$$\delta(n,t+1)=\frac{A^2-\psi_0}{A}\delta(n,t)+C[\langle\langle\delta(n,t)\rangle\rangle-\delta(n,t)] , \tag{A4}$$

or, taking the Fourier transform,

$$\delta(k,t+1)=\frac{A^2-\psi_0}{A}\delta(k,t)+C[\cos(k)-1]\delta(k,t) . \tag{A5}$$

The algorithm is unstable if $|\delta(k,t+1)|>\delta(k,t)|$ for some k, and, as we increase C (at fixed A), the first mode to go unstable is $k=\pi$ (alternating pattern). This occurs when

$$-1>\frac{A^2-\psi_0}{A}-2C , \tag{A6}$$

so that the nonconserved algorithm is linearly unstable if

$$C>0.5+\frac{A^2-\psi_0}{2A} . \tag{A7}$$

We can now use the $\delta(n,t+1)$ $[\equiv\delta'(n,t)]$ for the nonconserved case; calculated in Eq. (A4), as an element of the corresponding equation for the conserved algorithm

$$\delta(n,t+1)=\delta'(n,t)-\langle\langle\delta'(n,t)-\delta(n,t)\rangle\rangle , \tag{A8}$$

or, taking the Fourier transform,

$$\frac{\delta(k,t+1)}{\delta(k,t)}=\frac{A^2-\psi_0}{A}[1-\cos(k)]+C\{2\cos(k)-1-[\cos(k)]^2\}+\cos(k) . \tag{A9}$$

Setting again $k=\pi$, we obtain that the algorithm becomes unstable when

$$-1>\frac{2(A^2-\psi_0)}{A}-4C-1 , \tag{A10}$$

or, equivalently,

$$C>\frac{A^2-\psi_0}{2A} . \tag{A11}$$

If we choose $A=1.3$ in Eq. (A1), then $\psi_0\approx0.9777$ and the instability occurs when $C>0.2824$.

Considering now the effect of angular displacements, we can assume, without loss of generality, that the uniform solution ψ_0 lies initially in the direction of the X component. In the linear approximation, this component will be unaffected by a small angular perturbation, while the new Y component (corresponding to the perturbation δ) satisfies equations similar to Eqs. (A4) and (A8), except that we need to substitute the factor $(A^2-\psi_0)/A$ with 1. Therefore, we obtain that the nonconserved algorithm is linearly stable against angular perturbations when $C<1$ (independently of A), while the angular stability of the conserved algorithm requires $C<0.5$. For $A=1.3$, the value used in the simulations, these constraints are weaker than the ones obtained above (treating the order parameter as a scalar), and can therefore be safely ignored.

*Present address: Department of Materials Science, University of Cincinnati, 404 Rhodes Hall, Cincinnati, OH 45221-0012.

[1] General overviews of the field can be found in H. Furukawa, Adv. Phys. **34**, 703 (1985); J. D. Gunton, M. San Miguel, and P. S. Sahni, in *Phase Transitions and Critical Phenomena,* edited by C. Domb and J. L. Lebowitz (Academic, New York, 1983), Vol. 8.

[2] B. D. Gaulin, S. Spooner, and Y. Morii, Phys. Rev. Lett. **59**, 668 (1987); R. Toral, A. Chakrabarti, and J. D. Gunton, *ibid.* **60**, 2311 (1988).

[3] K. Kawasaki and T. Ohta, Physica A **118**, 175 (1983), and references therein.

[4] A. J. Bray and K. Humayun, J. Phys. A **23**, 5897 (1990).

[5] A. J. Bray, Phys. Rev. Lett. **62**, 2841 (1989).

[6] A. J. Bray, Phys. Rev. B **41**, 6724 (1990).

[7] A. Coniglio and M. Zannetti, Europhys. Lett. **10**, 575 (1989).

[8] M. Mondello and Nigel Goldenfeld, Phys. Rev. A **42**, 5865 (1990).

[9] M. Mondello and Nigel Goldenfeld, Phys. Rev. A **45**, 657 (1992).

[10] Fong Liu, M. Mondello, and Nigel Goldenfeld, Phys. Rev. Lett. **66**, 3071 (1991).

[11] H. Toyoki, J. Phys. Soc. Jpn. **60**, 1433 (1991).

[12] A. Bray and S. Puri, Phys. Rev. Lett. **67**, 2670 (1991).

[13] (a) H. Toyoki, Phys. Rev. B **45**, 1965 (1992); (b) F. Liu and G. F. Mazenko, *ibid.* **45**, 6989 (1992).

[14] A. J. Bray and K. Humayun, Phys. Rev. Lett. **68**, 1559 (19920.

[15] A. Coniglio, Y. Oono, A. Shinozaki, and M. Zannetti, Europhys. Lett. **18**, 59 (1992).

[16] For a review of the cell-dynamics method, see Y. Oono and A. Shinozaki, Forma **4**, 75 (1989), and references therein.

[17] All our measurements involve an ensemble averaging over initial conditions and, for space- or wave-vector-dependent quantities, an average over all directions.

[18] C. Yeung, Phys. Rev. Lett. **61**, 1135 (1988).

[19] A. Shinozaki and Y. Oono, Phys. Rev. Lett. **66**, 173 (1991).

[20] K. Kawasaki, Phys. Rev. A **31**, 3880 (1985) and references therein.

[21] We thank Martin Grant for encouraging us to pursue this analogy. A related issue is the spinodal decomposition of a crystal surface to form hill and valley structures; see J. Stewart and N. Goldenfeld, Phys. Rev. A **46**, 6505 (1992).

[22] See, for example, B. Nienhuis, in *Phase Transition and Critical Phenomena,* edited by C. Domb and J. L. Lebowitz (Academic, New York, 1987), Vol. 11, and references therein.

[23] We should stress from the outset that while the correspondence between the equilibrium statistical mechanics of the SOS and XY models is based on a well-defined mathematical mapping between the corresponding partition functions, it is qestionable whether a formal extension of this mapping to the nonequilibrium case actually exists. At this stage, the proposed correspondence has an essentially heuristic character, grounded on the guiding principle of universality, as discussed below in the main text, and the presently available empirical and numerical evidence.

[24] The situation is in fact more complicated since, on a (fully) roughened interface, points that are close in space can have large interfacial separations, so that nonlocal mas exchanges are possible and the conservation law for the interface can only be defined globally.

[25] W. W. Mullins, J. Appl. Phys. **28**, 333 (1956).

[26] W. W. Mullins, J. Appl. Phys. **30**, 77 (1959).

[27] J. Villain, Europhys. Lett. **2**, 531 (1986).

[28] Martin Grant, Phys. Rev. B **37**, 5705 (1988).

[29] Changes may occur occasionally in the early stages of the evolution, when we can have $\Delta\theta \approx \pi$.

[30] T. J. Newman, A. J. Bray, and M. A. Moore, Phys. Rev. B **42**, 4514 (1990).

[31] Y. Oono and S. Puri, Phys. Rev. A **38**, 434 (1988).